Journal of Power Sources 230 (2013) 282–289

Contents lists available at SciVerse ScienceDirect

Journal of Power Sources

journal homepage: www.elsevier.com/locate/jpowsour

Hydrogen sulfide-resilient anodes for molten carbonate fuel cells

Hoang Viet Phuc Nguyen [a,b], Shin Ae Song [b,**], Dongho Seo [b], Jonghee Han [b], Sung Pil Yoon [b], Hyung Chul Ham [b], Suk Woo Nam [b], Mohd Roslee Othman [c], Jinsoo Kim [a,*]

[a] Department of Chemical Engineering, Kyung Hee University, 1 Seocheon-dong, Giheung-gu, Yongin, Gyeonggi-do 446-701, Republic of Korea
[b] Fuel Cell Research Center, Korea Institute of Science and Technology, Hwarangno 14-gil 5, Seongbuk-gu, Seoul 136-791, Republic of Korea
[c] School of Chemical Engineering, Universiti Sains Malaysia, 14300 Nibong Tebal, Penang, Malaysia

HIGHLIGHTS

- Systematical study of Fe introduction into conventional Ni–Al anode.
- Improvement of creep resistance and tolerance to H_2S.
- High long term stability of cell with low voltage loss of ca. 5 mV.
- Significant recovery of the modified anodes from H_2S poisoning effect.

ARTICLE INFO

Article history:
Received 29 September 2012
Received in revised form
10 December 2012
Accepted 12 December 2012
Available online 31 December 2012

Keywords:
Molten carbonate fuel cell
Anode
Creep resistance
Electro-chemical performance

ABSTRACT

Nickel aluminum (Ni–Al) alloy anodes have become the preferred choice in anode material and have received widespread attention in molten carbonate fuel cell (MCFC) research due to their high durability and effectiveness in resisting creep of stack loadings. They are, however, susceptible to hydrogen sulfide (H_2S) poisoning, which results in pore compression and rapid reduction of active sites for the electro-catalytic reaction. In this work, iron is introduced into a conventional Ni–Al anode to improve the creep resistance and tolerance to H_2S. Anodes containing 30 wt.% Fe have a low creep strain of ca. 3%, but their creep resistance is much better than that of standard anodes. Single cells operated stably over 1000 h with a low voltage loss of ca. 5 mV. When exposed to H_2S, the modified anode exhibited excellent recovery from the poisoning effect.

1. Introduction

Ni–Cr is a state-of-the-art anode material for modern MCFC systems [1]. Ni–Cr also reportedly, however, 'consumes' electrolytes when lithiation occurs in the system. Therefore, Ni–Al has become the preferred choice in anode material selection and has received widespread attention due to its high durability and effectiveness in resisting the creep of stack loadings [2–7].

Because MCFCs have high operating temperatures (923 K), natural gas, coal gas and bio-fuels are some of the fuel options for anodes. These fuels contain a variety of contaminants and impurities, such as sulfur compounds (H_2S, COS, etc.), halides, tars, dust, ammonia, and soloxanes. It is known that H_2S is the most harmful impurity for cell performance. The total sulfur content of pipeline natural gas is on the order of 10–80 ppm, with 4 ppm H_2S and 4 ppm mercaptans [8]. The hydrogen sulfide concentration in bio-fuels such as landfill gas or anaerobic digestion product gas can be as much as 200 ppm [9,10]. The product gases from coal gasification typically contain 0.1–1% or more H_2S [11]. Before they are used in MCFCs, first stage cleanup processes are applied, during which the tolerance limit of H_2S concentration for MCFCs varies from 0.01 ppm to less than 10 ppm [12–14]. The tolerance limit of H_2S, however, depends on the technology, operating conditions and hydrogen gas concentration. If the cleanup processes are not properly completed, higher amounts of hydrogen sulfide gas (>10 ppm) can severely poison the anode material.

Due to a very low dissociation barrier of Ni with H_2S, the rapidly strong absorption of H_2S on an anode surface has been found [15,16] to block the active sites, cover the pore network, increase cell polarization, change the wettability of the electrolyte, and thus degrade the cell performance [17–20]. In the presence of H2S, the reactions that occur in the electrolyte and anode are as follows:

With electrolyte

* Corresponding author. Tel.: +82 31 201 2492; fax: +82 31 204 8114.
** Corresponding author. Tel.: +82 2 958 5295; fax: +82 2 958 5199.
E-mail addresses: shinaesong@kist.re.kr (S.A. Song), jkim21@khu.ac.kr (J. Kim).

0378-7753/$ – see front matter © 2012 Elsevier B.V. All rights reserved.
http://dx.doi.org/10.1016/j.jpowsour.2012.12.077

$$H_2S + CO_3^{2-} \rightarrow H_2O + CO_2 + S^{2-} \quad (1)$$

$$H_2S + CO_3^{2-} + 3H_2O \rightarrow SO_4^{2-} + CO_2 + 4H_2 \quad (2)$$

with anode

$$Ni + H_2S \rightarrow NiS + H_2 \quad (3)$$

$$Ni + S^{2-} \rightarrow NiS + 2e^- \quad (4)$$

Under MCFC working conditions, Al in the Ni-based matrix diffuses out from the anode surface to react with water vapor and form an oxide layer. This alumina layer functions as a protective layer and inhibits impurity invasions from materials such as oxygen, carbon or sulfur [21–23]. It is not sufficient, however, to stop the effects of H_2S poisoning. It is well-known that Fe_2O_3 is an excellent desulfurization reagent for H_2S removal from waste gas or natural gas at high temperatures [24]. The effect of Fe_2O_3 when water is present during H_2S regeneration has been discussed [25,26], and studying the effects of Fe incorporated into conventional MCFC anodes on the resistance to H_2S poisoning is meaningful.

In this work, a Ni–Al–Fe alloy anode is prepared. Fe is introduced not only because of its excellent desulfurization capability, but also because of its ability to facilitate hydrogen diffusion [27–30]. In order for the newly fabricated Ni–Al–Fe alloy anode to function properly, it must improve creep resistance, tolerate H_2S poisoning and improve overall electro-chemical performance. All of these factors are evaluated using a single cell test.

2. Experimental

2.1. Anode fabrication

The raw material for anode tape casting was prepared by mixing Ni-5 wt% Al powder (Twin Energy, >99%, 3–5 μm) with various contents (10–30 wt.%) of Fe powder (>99%, 3–5 μm) and Ni powder (Inco type 255, >99%, 3–5 μm). The green anode sheet prepared by tape casting was sintered at 1223 K under an H_2/N_2 (10/90) atmosphere for 0.5 h to prepare the alloy. The anode without the addition of Fe was designated as 0Fe sample; the anodes with 10 wt.% and 30 wt.% Fe content were designated as 10Fe and 30Fe, respectively. The basic characteristics of the as-prepared anodes were characterized using X-ray diffraction (XRD, MiniFlex II, Rigaku), a scanning electron microscope combined with an energy dispersive spectrometer (ESEM/EDS, XL300, Philip) and an electron probe micro-analyzer (EPMA, JXA-8500F, Jeol). The process of the American Society for Testing and Materials (ASTM C373-88) was followed when testing the sample porosity.

2.2. Creep test system

Creep resistance of the sintered anode Ni–Al–Fe was evaluated in a creep test system designed to control anode chamber conditions. A sintered anode of size ($1 \times 1 \times 0.07$) cm^3 was inserted between the stainless steel plates on the support rod in the lower space of the creep test equipment. After heating from room temperature, the temperature in the sample chamber was maintained at 923 K under anode gas conditions (H_2:CO_2 humidified with H_2O at 323 K) for several hours to allow for the necessary thermal expansion inside the support rod and the ceramic rod. One hundred psi of air was applied to the sintered anode for 100 h, and the thickness variation of the electrode was measured using the micro-thickness gauge attached to the equipment. Creep strains of the as-prepared samples were calculated from the creep ratio equation [2,3].

2.3. Single cell test

Single cells using sintered Ni–Al–Fe anodes with an effective area of 100 cm^2 were operated at 923 K. A lithiated NiO cathode, α-$LiAlO_2$ matrix, and the $(Li_{0.7}/K_{0.3})_2CO_3$ electrolyte sheet prepared by tape casting were used. A mixture of air: CO_2 = 70:30 was supplied as the cathode gas, and a mixture of H_2:CO_2:H_2O = 72:18:10 was used as the anode gas. The H_2O content of the anode gas was supplied using an evaporator humidified at 323 K. The flow rate of the reaction gas was fixed to maintain a fuel–air ratio of 0.4. The open-circuit voltage (OCV), current density–voltage (*I–V*) characteristics, ohmic resistance and amount of nitrogen cross-over were measured to evaluate the performance of the single cell. The cell performance was evaluated by measuring the cell voltage at various current densities. A DC current was applied to the cell using an electric loader (ELTO DC Electronics Co., ESL300Z). To analyze the electrode polarization and ohmic resistance, electro-chemical impedance analysis (EIS) was carried out in the open circuit voltage condition (OCV) using a Solartron S11287 and 1260B. The frequency range of the present EIS experiment was 10,000–0.01 Hz.

2.4. Short-term H_2S poisoning test

After the single cell reached stabilization, 20 ppm of H_2S (H_2 balance) was introduced in the anode gas for 100 h under loading at 150 mA cm^{-2} of current density. Then, H_2S feeding to the anode was stopped, and the single cell was maintained in an OCV state at 150 mA cm^{-2} of current density for 72 h, the so-called "regeneration" step. Then, H_2S concentrations of 50 ppm, 100 ppm and 150 ppm were fed into the anode gas stream using the same settings. The single cell performance was monitored and recorded. The single cell polarization was measured by an electro-chemical impedance analysis after each step at open circuit voltage (OCV) conditions. In post-test analysis, the samples were examined using an ESEM/EDX, EPMA and ASTM C373-88.

2.5. Out of cell test

Pure Ni and Ni-50 wt.% Fe samples of small-size ($1 \times 2 \times 0.07$) cm^3 were exposed to a 100 ppm H_2S/H_2 gas stream either without water vapor (the dry condition) or with water vapor (the wet condition) in a tubular reactor at 923 K for 100 h. In the wet condition, 10 vol.% of water vapor was supplied into the reactor with the simulated anode reactant gas in the MCFC. The anode surface was analyzed by EPMA after the test.

3. Results and discussion

Porosity and pore diameter are important factors that significantly affect mass transfer and cell performance [1]. The porosity and mean pore diameter of the sintered anodes with varying iron contents are shown in Table 1. The microstructural properties of the modified anodes are similar to those of the conventional anode (0Fe). It was expected that the mass transfer process would not change after modification with Fe. The XRD patterns for the samples at wide (Fig. 1a) and narrow (Fig. 1b) angles are presented

Table 1
The physical properties of conventional and modified anodes used in this work.

Sample	Porosity (%)	Pore diameter (μm)
0Fe (Ni-40 wt.% NiAl)	62	3
10Fe (Ni-40 wt.% NiAl-10 wt.% Fe)	65	3.3
30Fe (Ni-40 wt.% NiAl-30 wt.% Fe)	63	3.4

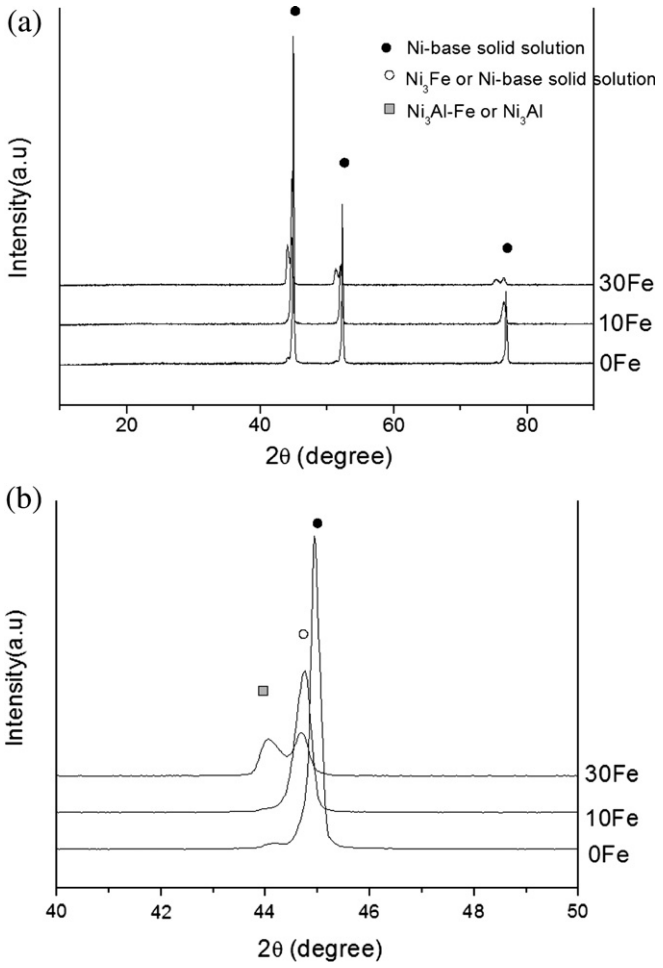

Fig. 1. X-ray diffraction pattern of as-prepared NiAl–*x*Fe anodes in (a) wide angle view and (b) narrow angle view.

in Fig. 1. After the addition of Fe, the specific peaks of the anode samples are shifted to a smaller theta angle because of the different atomic radii of Fe (140 pm) [31], Ni (135 pm) [31,32] and Al (125 pm) [31,33]. According to Bragg's law, the replacement of Fe into the Ni–Ni matrix or the Ni–Al matrix would increase the

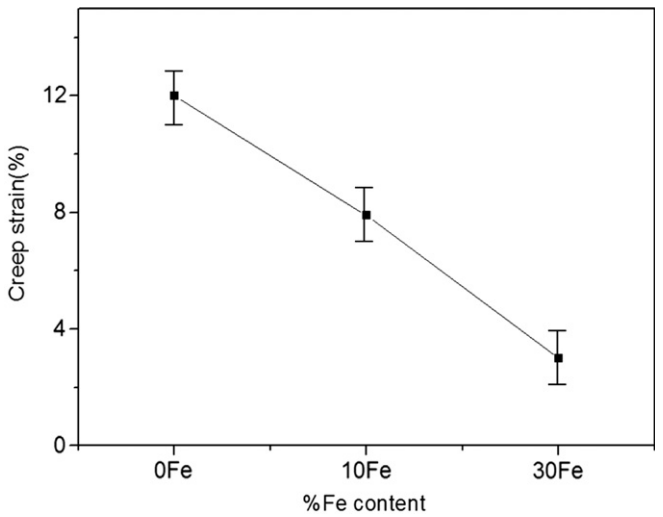

Fig. 2. Creep strain behavior of NiAl–*x*Fe anodes at 923 K over 100 h under loading of 100 psi of a mixture gas (H_2, CO_2) humidified with water at 323 K.

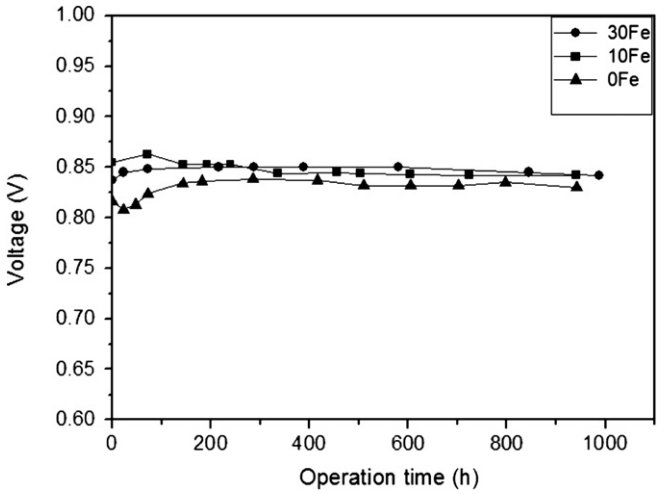

Fig. 3. Single cell performance of NiAl–*x*Fe anodes as a function of operation time. The operation temperature and current density were fixed at 923 K and 150 mA cm^{-2}, respectively.

distance between the two atoms, resulting in a shifting of the peak to a smaller theta angle (Fig. 1b). Anode samples with 10 wt.% Fe exhibited a disordered Ni_3Fe phase. As the Fe content is increased to 30 wt.%, a less disordered Ni_3Al–Fe phase is identified.

The phase stability of ordered Ni_3Al at high temperatures of up to 1603 K has been reported previously [34]. The activation energy of Fe diffusion into Ni_3Al has been found to be lower than that of Ni into Ni_3Al [35,36] and Fe entering the Al sub-lattice of ordered Ni_3Al [37,38]. The existence of an order/disorder transition region for Ni_3Al–Ni_3Fe with Fe content below 25 wt.% in the temperature range 200–1800 K [39] or with a disordered Ni_3Fe phase occurring at ca. 776 K [40,41] has been reported by several researchers.

In this work, different amounts of Fe were found to create different phases, giving rise to different levels of creep resistance, as shown in Fig. 2. Samples with higher Fe content exhibited better creep resistance due to the diffusion of Fe into the Ni–Al system, which led to solid solution formation and improved the yield strength of the material [34–37]. When the Fe content was increased, the combination of an ordered Ni_3Al–Fe phase and a disordered Ni_3Fe phase enhanced the strength of the grain boundary, which significantly depressed the flow stress diffusion.

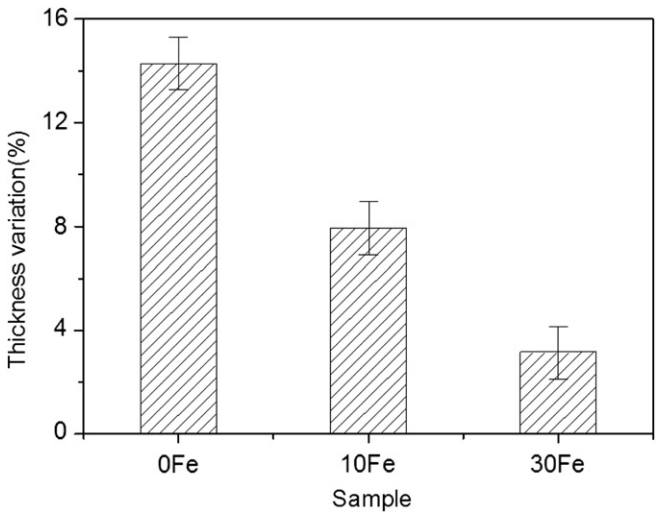

Fig. 4. Thickness variation behavior of the modified anodes after a single cell test at 923 K for 1000 h.

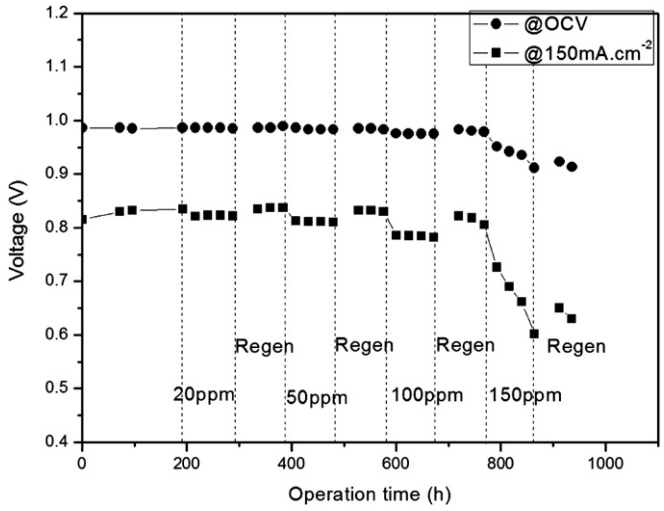

Fig. 5. Single cell performance of 0Fe anodes under H_2S short-term poisoning as a function of operation time and H_2S concentration.

This resulted in a decrease of the bending moment at necked grains known to affect the creep strain behavior of porous anodes [2,3].

Single cell performances using three different anode samples are shown in Fig. 3. All single cells achieved stable voltage gain greater than 0.8 V at 150 mA cm^{-2}. The instability in the initial stage of operation is normal and was due to electrolyte redistribution in the matrix and the electrode, the lithiation reaction at the cathode side and creep loading at the anode side [42,43]. The voltage losses in the 10Fe and 30Fe single cells were 3 mV per 1000 h and 5 mV per 1000 h, respectively. These values are significantly lower than that for 0Fe (20 mV per 1000 h). In post-test analysis, the variations in the thickness of the anodes were analyzed, and the results are shown in Fig. 4. It is obvious that the modified anodes show less variation than the non-modified anodes, meaning that the high creep-resistant anode maintained its own pore structure during cell operation. Therefore, long-term stability with lower voltage loss was reasonably achieved.

The effect of H_2S on single cell performance with a conventional anode is shown in Fig. 5. Different H_2S concentrations were supplied to the anode during the test. It is clear that the presence of H_2S in the cell degraded the overall cell voltage. At higher concentrations, greater voltage drop is observed. Cell performance after the introduction of H_2S consisted of two stages. Immediately after the introduction of H_2S, the voltage drops rapidly, followed by stabilization over 100 h of operation. The rapid voltage drop is due to instantaneous H_2S physical absorption onto the Ni surface without nickel sulfide formation [44]. This poisons the active sites, resulting in the immediate decrease in performance. The stabilization of the cell voltage in the second stage is observed [17,20] when a hot H_2 stream is continuously fed into the cell, the sulfur is partially removed, and the anodes are regenerated. Although recovery of cell performance is achieved after supplying the cell with cleaner fuel, lower voltages are obtained due to the poisoning effect at the anode, as described in Equations (3) and (4) above. As the operation progresses, stable chemical bonding of Ni and S^{2-} anions creates nickel sulfide compounds [45–47] at the active sites, causing the voltage to degrade further. The severity of the poisoning on the anode depends on the H_2S/H_2 ratio, as observed in this study and reported previously [20,48]. Therefore, as the H_2S concentration is increased, greater voltage loss is observed. At 150 ppm H_2S, a marked cell voltage dropped is observed. This decrease is not recovered with the supply of cleaner H_2 fuel.

The sulfur distribution on the conventional anode surfaces measured using EPMA mapping after heat-treatment at 923 K for 100 h in an H_2 atmosphere with 100 ppm H_2S is shown in Fig. 6. The first image (top left) identifies two possible phases in the conventional Ni–Al anode with bright and dark patterns. The dark pattern represents Al-rich sites (the second image in a clockwise direction), whereas the bright pattern represents the Ni–Al phase with Al-lean sites (third image in a clockwise direction). Higher amounts of sulfur were deposited on the bright sites (Al-lean sites), while less sulfur was deposited on the dark sites (Al-rich sites). This is reportedly due to the fact that the adsorption and dissociation rates of H_2S on Al_2O_3 are much slower because of the large band gap in the oxide, resulting in difficult mixing with the H_2S orbital [49]. It is possible that the alumina formed on the Ni–Al alloy inhibited the

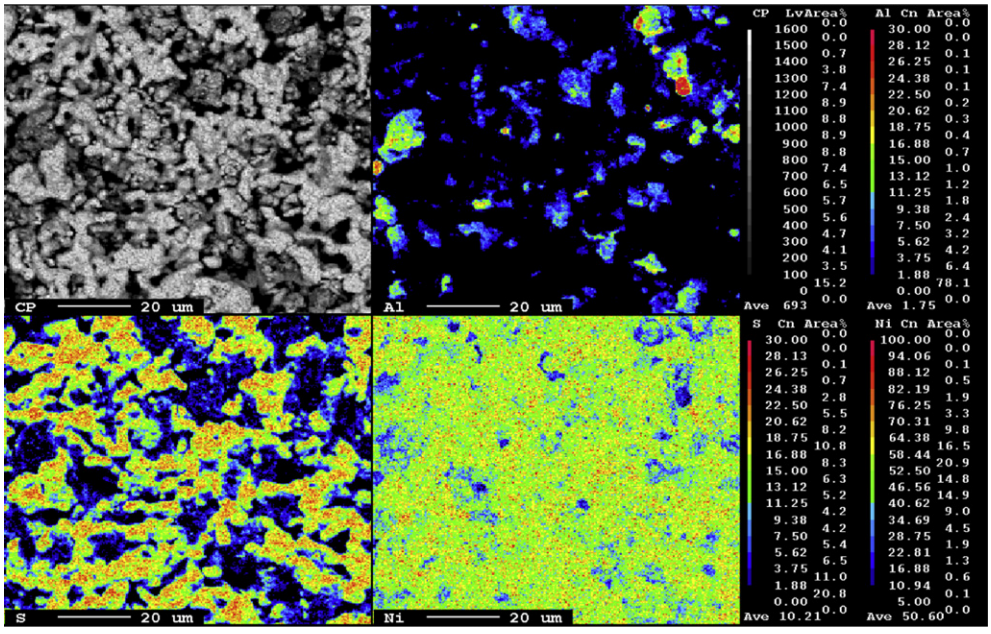

Fig. 6. EPMA mapping images of a 0Fe sample heat-treated at 923 K for 100 h in an H_2 atmosphere with 100 ppm H_2S.

interaction of Ni and S and the penetration of S into the Ni matrix under the poisoning state. In the MCFC anode, the Al diffused on the anode surface becomes an Al_2O_3 layer [23]. This layer depressed the interaction of Ni and S and prevented severe poisoning of the active sites. This explains the steady cell performance even after degradation by H_2S at low concentrations (Fig. 5). It is found that Al in the Ni–Al alloy played an important role in depressing the H_2S poisoning effect. Depressing the H_2S poisoning effect by the mere addition of Al was not sufficient, however, especially when the concentration of H_2S was high.

Cell performance using modified anodes with Fe under short-term H_2S poisoning is shown in Fig. 7(a and b). The cell voltage performance after H_2S exposure is not different from that of the conventional cell. The level of the voltage drop in the former cell using the modified anodes is much lower than that of the latter cell, however. A marked difference is observed at 150 ppm H_2S. The cell maintains its performance over 100 h of operation. The voltage drop as a function of H_2S concentration is presented in Fig. 8, which also compares the voltage drop from the two types of cells. The voltage drop for the 10Fe and 30Fe samples were 35 mV and 38 mV at H_2S concentrations of 100 ppm, respectively, whereas the voltage drop for the standard anode cell was 45 mV. At a higher H_2S concentration of 150 ppm, the modified anode cells suffered voltage drop of ca. 50–60 mV, while the voltage drop in the conventional cell was not obtainable because the voltage read 0 V as soon as 150 ppm H_2S was introduced. This shows that

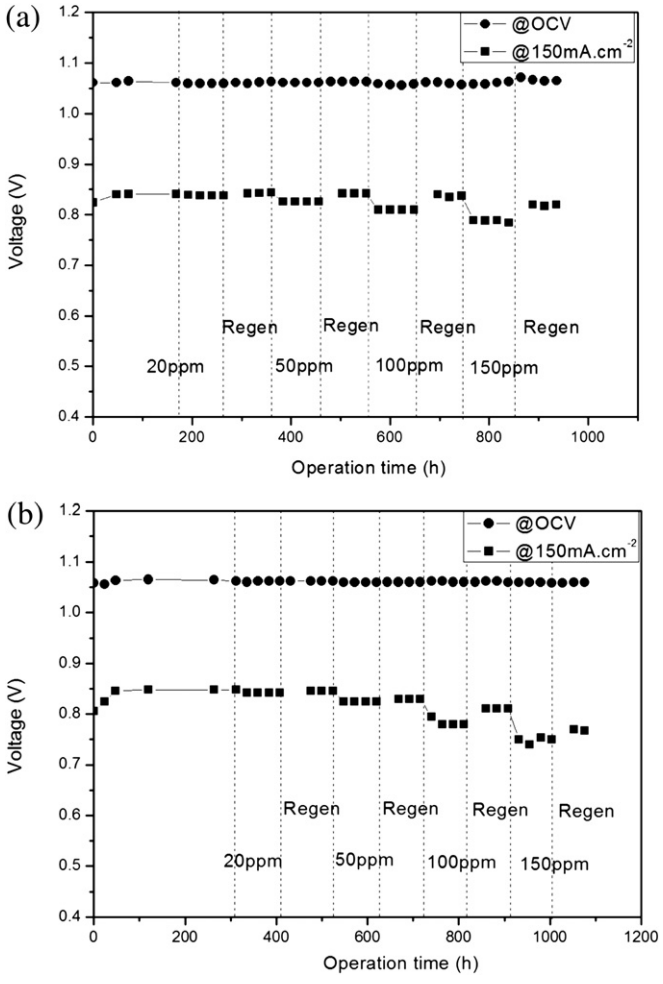

Fig. 7. Single cell performance of (a) a 10Fe anode and (b) a 30Fe anode under H_2S short-term poisoning as a function of operation time and H_2S concentration.

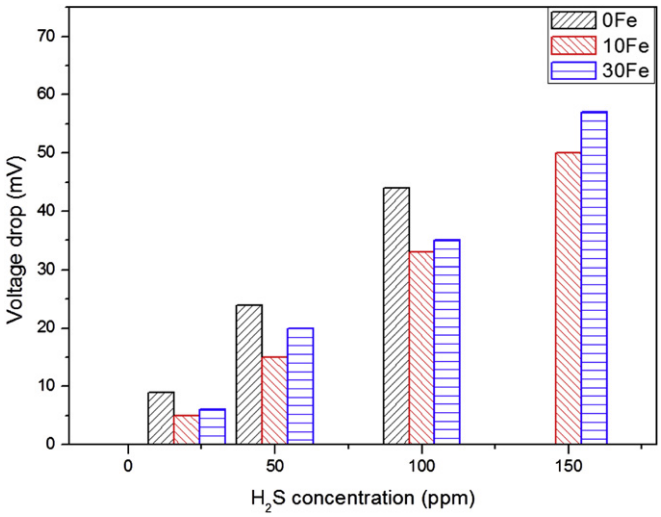

Fig. 8. Voltage decreases of cells with 0Fe, 10Fe and 30Fe anodes at different H_2S concentrations after short-term H_2S poisoning.

the modified anode could tolerate H_2S poisoning even at high concentrations.

During cell operation, the Fe in the anode was easily oxidized into Fe_xO_y as Al diffused on the anode surface to form an Al_2O_3 layer [23]. The oxygen partial pressure for the oxide formation of Fe (10^{-8}–10^{-9} Pa at 923 K) was relatively low [50]. In the MCFC anode, oxidizing Fe was even easier in the presence of H_2O and CO_2. Iron oxide has been applied in desulfurization processes at high temperatures [24,51,52]. Ion sulfide has also been used as an active catalyst for H_2S decomposition in rich H_2S gas streams or under the presence of high concentrations of H_2O and low concentrations of O_2 [53,54]. Sasaoka et al. [25,26] indicated that H_2O directly contributed to the oxidation of iron oxides and the presence of O_2 accelerated oxidative regeneration. Devianto et al. [18] found that higher water concentrations can decrease the H_2S poisoning effect.

In this work, a sintered Ni-50 wt.% Fe sample was exposed to 100 ppm H_2S at 923 K for 100 h under both dry and wet conditions in order to study the interaction between Ni–Fe and H_2S. The dispersion of sulfur on the surfaces of Ni-50 wt.% Fe was examined using EPMA, and the results are displayed in Fig. 9. More sulfur was detected in the sample exposed to H_2S in the dry condition than that in the wet condition. Practically, water vapor of 10 vol.% was supplied with a hot, rich H_2 gas stream to prevent carbon coking. The results from the out of cell tests under the wet conditions were similar to those found in practice. Possible reactions explaining the reduction of sulfur on the anode surface in the Fe modified anode are as follows:

$$Fe_xO_y + yH_2S \rightarrow Fe_xS_y + yH_2O \quad (5)$$

$$Fe_xS_y + (z+2y)H_2O \leftrightarrow Fe_xO_Z + ySO_2 + (z+2y)H_2 \quad (6)$$

First, S is rapidly dissociated from H_2S, and the former is adsorbed onto the iron oxide at the anode according to reaction (5) [24,51]. Fe_xS_y then reacts with water vapor to produce SO_2 and returns to its initial state as iron oxide, as described by the reversible reaction (6). It was apparent that iron sulfide was oxidized back to iron oxide more favorably under the wet conditions than under the dry conditions. As a result, the amount of S coverage on the modified anode surface was significantly reduced, providing a reasonable explanation for the positive effect of Fe addition on H_2S poisoning.

(a) Ni-50Fe - dry condition

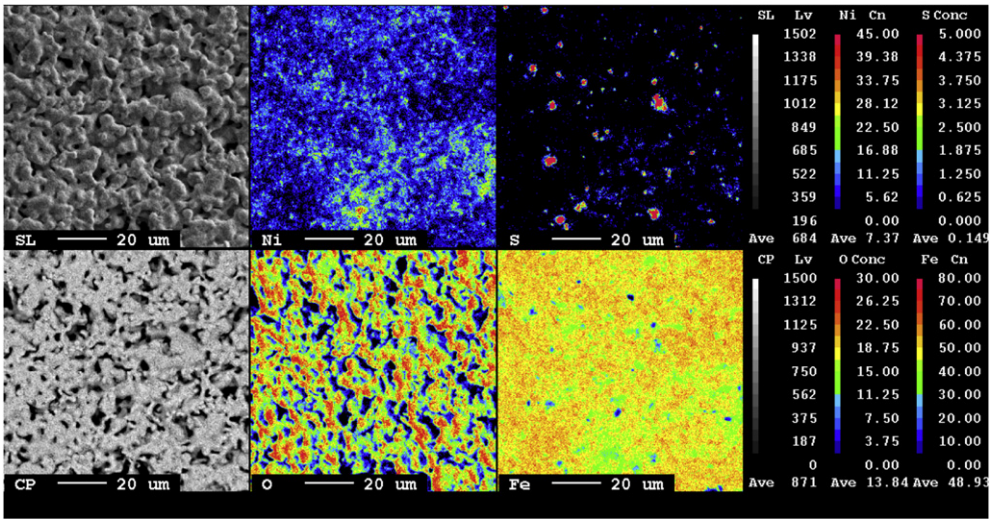

(b) Ni-50Fe - wet condition

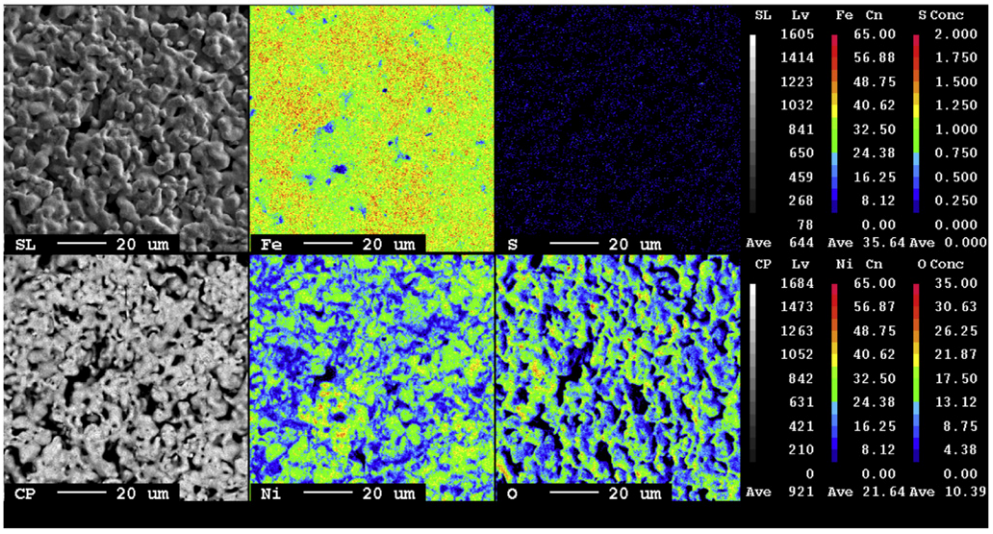

Fig. 9. EPMA mapping images of (a) Ni-50 wt.% Fe plate heat-treated under dry conditions and (b) Ni-50 wt.% Fe plate heat-treated under wet conditions with 100 ppm H_2S at 923 K for 100 h.

10Fe (50wt.%Ni-40wt.%Ni5Al-10wt.%Fe)- wet condition

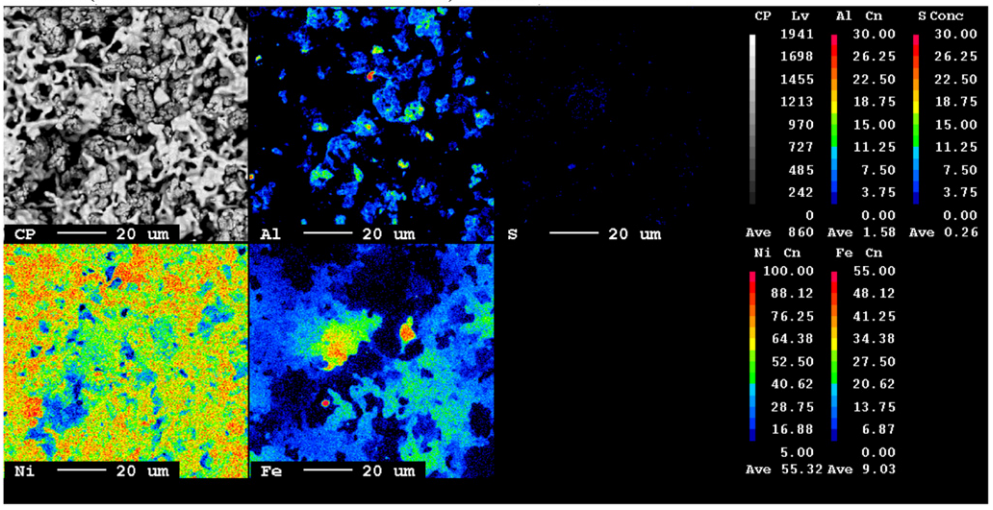

Fig. 10. EPMA mapping images of 10Fe anodes heat-treated under wet conditions with 100 ppm H_2S at 923 K for 100 h.

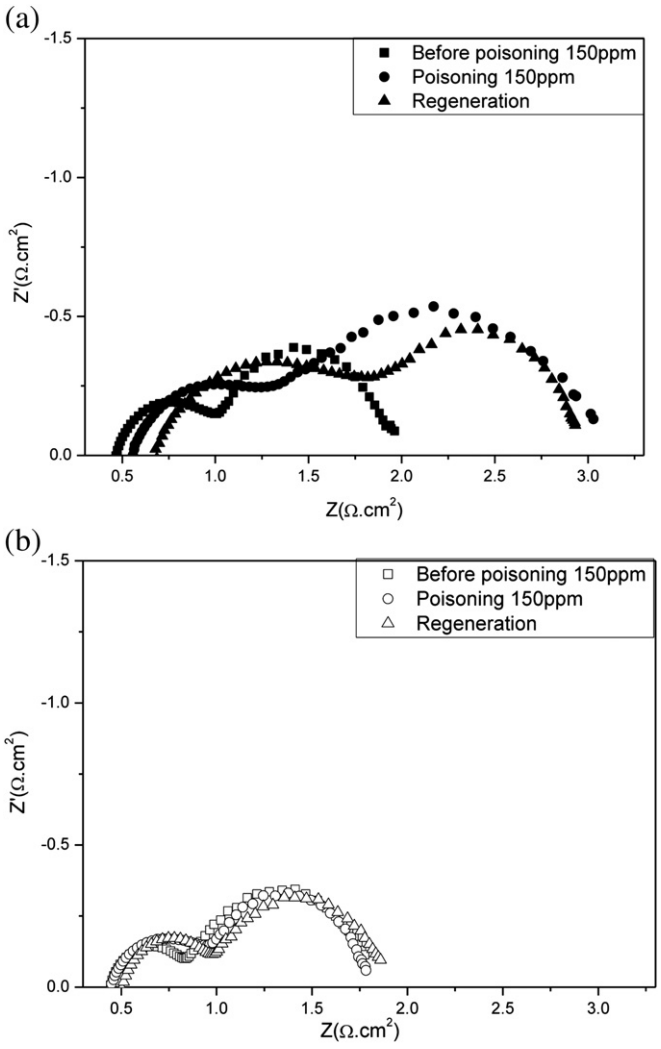

Fig. 11. Electrochemical impedance spectra in cells with (a) 0Fe and (b) 30Fe anodes under three conditions: before poisoning, during poisoning (with 150 ppm H_2S) and during regeneration during the single cell test.

The sulfur distribution on the 10Fe anode exposed to 100 ppm H_2S at 923 K for 100 h under the wet conditions is shown in Fig. 10. Little sulfur is detected in the sample, confirming the earlier results that sulfur poisoning could be successfully prevented if Fe is incorporated into the standard anode.

Fig. 11 shows the cell polarizations for the 0Fe and 30Fe anodes in three different conditions: before poisoning at 150 ppm, during the poisoning stage and during the regeneration stage. Since the system consisted of an identical matrix (i.e., the electrolyte and cathode were in a single cell), the variation in cell polarization was presumably caused by changes in anode polarization. Generally, the EIS curve shows two semi-circles: the first semi-circle relates to the charge transfer resistance, and the other represents the mass transfer resistance [55,56]. The polarizations of the cells show similar behaviors: they increase during the poisoning period and decrease back to the pre-poisoning position during regeneration. As shown in Fig. 11(a), significant increases in both charge transfer resistance and mass transfer resistance in the 0Fe anode cell were observed. When H_2S was introduced together with the anode reactant gas, the H_2S was immediately absorbed on the surface of the 0Fe anode, poisoning the active sites and causing the charge transfer resistance to increase. The anode pores were also blocked due to the formation of nickel sulfide compounds [15–20,57], resulting in an increase in the mass transfer resistance. Despite regeneration, the polarization curve did not return to its initial condition (i.e., before poisoning).

For the 30Fe anode, the polarization after H_2S poisoning was much smaller for the 0Fe anode, as shown in Fig. 11(b). The polarization after regeneration was also insignificant. This is further evident by the fact that Fe-modified anodes are capable of tolerating H_2S poisoning by effectively decomposing the H_2S and maintaining the anode structural integrity.

The surface morphologies of the 0Fe and 30Fe anodes under several conditions are shown in Fig. 12. The SEM images of the 0Fe and 30Fe anodes prior to the cell test are shown in Fig. 12(a) and (d), respectively. The SEM images of the 0Fe and 30Fe anodes after cell operation without H_2S poisoning are shown in Fig. 12(b) and (e), respectively. The SEM images and the EDS results for the 0Fe and 30Fe anodes after cell operation with H_2S poisoning are shown in Fig. 12(c) and (f), respectively. As shown in Fig. 11(b) and (e), the 0Fe

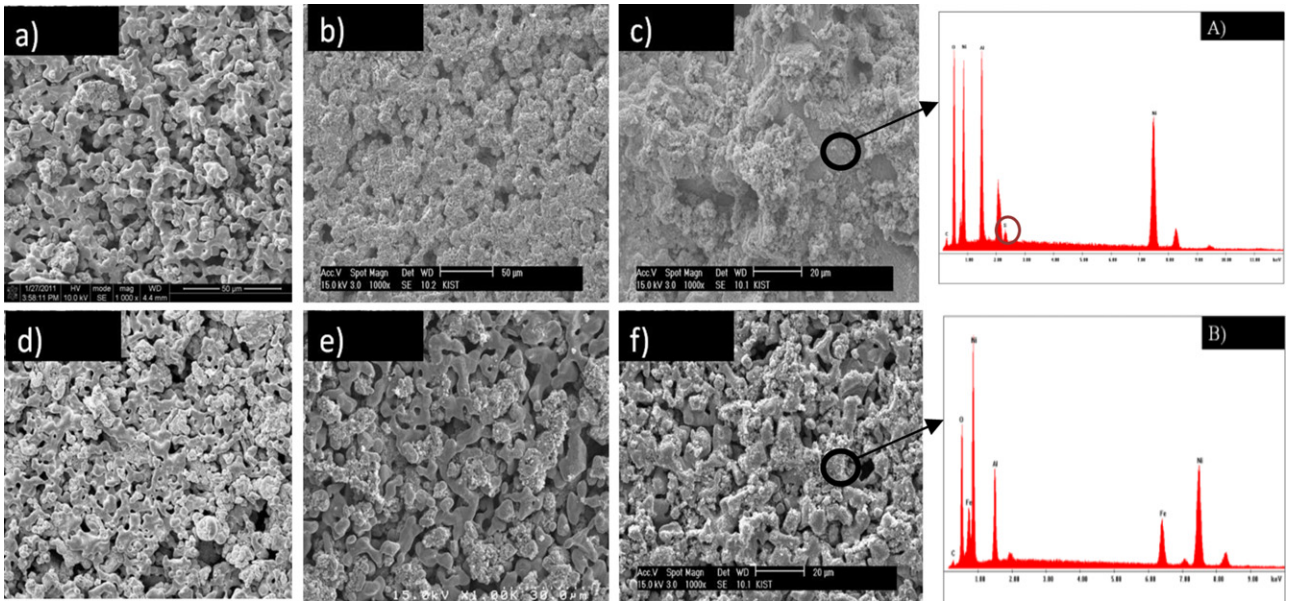

Fig. 12. SEM images of 0Fe and 30Fe: (a), (d) before the single cell test; (b), (e) after the single cell test without H_2S poisoning; (c), (f) after the single cell test with H_2S poisoning.

anode suffered severe creep loading compared to the 30Fe anode after cell operation. The pore structural integrity of the modified anode was maintained despite H_2S poisoning, as shown in Fig. 12(c), while the pore structure of the standard anode presented in Fig. 12(f) is severely collapsed. The EDS results show that S was detected in the 0Fe sample after cell operation with H_2S poisoning. S was not detected in the 30Fe sample after cell operation with H_2S poisoning. The collapse phenomenon of the pore structure in the 0Fe anode after cell operation with H_2S poisoning was caused by the formation of nickel sulfide. The reductions in the Ni grain boundary strength and tensile strength due to sulfur segregation to the Ni grain boundary resulting in easy cracking have been reported previously [58]. For the modified anode, however, the pore structure was maintained because nickel sulfide was not formed due to the catalytic ability of iron oxide to decompose and oxidize H_2S to form SO_2. The SEM and EDS results confirmed the EIS behaviors of single cells using 0Fe and 30Fe anodes, respectively (Fig. 11).

4. Conclusions

Despite being susceptible to the poisoning effect of H_2S, anodes containing Fe are found to be more resilient than the anodes that did not contain Fe. The Fe anodes recover more quickly and deposit less sulfur over the cell test operation period. The presence of Fe in the anode samples significantly improves the creep resistance, leading to an overall improvement in cell test performance. Therefore, the Ni–Al–Fe anodes proposed in this study are recommended for MCFCs that are fueled by hydrogen containing traces of sulfur compounds such as hydrogen sulfide or carbonyl sulfide.

Acknowledgments

This research was supported by the Renewable Energy R&D Program of the Korea Institute of Energy Technology Evaluation and Planning (KETEP) grant funded by the Ministry of Knowledge Economy, Republic of Korea (No. 20113030030040).

References

[1] J. Larminie, A. Dicks, Fuel Cell System Explained, second ed., John Wiley & Sons Inc., 2006.
[2] Y.S. Kim, K.Y. Lee, H.S. Chun, J. Power Sources 99 (2001) 26–33.
[3] G.B. Kim, Y.J. Moon, D. Lee, J. Power Sources 104 (2002) 181–189.
[4] C.A. Hippsley, J.H. Devan, Acta Metall. 37 (1989) 1485–1496.
[5] C.T. Liu, C.L. White, J.A. Horton, Acta Metall. 33 (1985) 213–229.
[6] T. Takasugi, O. Izumi, N. Masahashi, Acta Metall. 33 (1985) 1259–1269.
[7] T. Takasugi, O. Izumi, Acta Metall. 33 (1985) 1247–1258.
[8] T. Watanabe, Y. Izaki, Y. Mugikura, H. Morita, M. Yoshikawa, M. Kawase, F. Yoshiba, K. Asano, J. Power Sources 160 (2006) 868–871.
[9] R.J. Spiegel, S.A. Thorneloe, J.C. Trocciola, J.L. Preston, Waste Manag. 19 (1999) 389–399.
[10] Roberto Bove, Piero Lunghi, J. Power Sources 145 (2005) 588–593.
[11] D.C. Dayton, M. Ratcliff, R. Bain, Fuel Cell Integration. A Study of the Impacts of Gas Quality and Impurities. Milestone Completion Report, NREL/MP-510–30298, 2001.
[12] Fuel Cell Handbook, seventh ed., EG&G Technical Services, Inc. under contract of US Department of Energy, 2004.
[13] G. Iaquaniello, A. Mangiapane, Int. J. Hydrogen Energy 31 (2006) 399–404.
[14] Supramaniam Srinivasan, Fuel Cells: From Fundamentals to Applications, Springer, 2006.
[15] Alfred B. Anderson, S.Y. Hong, Surf. Sci. 204 (1988) L708–L712.
[16] I. Chen, D.-W. Shiue, Ind. Eng. Chem. Res. 27 (1988) 1391–1396.
[17] H. Devianto, S.Y. Yoon, S.W. Nam, J. Han, T.-H. Lim, J. Power Sources 159 (2006) 1147–1152.
[18] H. Devianto, E. Simonetti, A. Moreno, F. Zaza, V. Cigolotti, Int. J. Hydrogen Energy 37 (2012) 19312–19318.
[19] N. Di Giulio, B. Bosio, V. Cigolotti, S.W. Nam, Int. J. Hydrogen Energy 37 (2012) 19329–19336.
[20] V. Cigolotti, S. McPhail, A. Moreno, S.P. Yoon, J. Han, S.W. Nam, T.H. Lim, Int. J. Hydrogen Energy 36 (2011) 10311–10318.
[21] M. Ziolek, J. Kujawa, O. Saur, J.C. Lavalley, J. Mol. Catal. A Chem. 97 (1995) 49–55.
[22] Y. Liu, K.Y. Chen, G. Lu, J.H. Zhang, Z.Q. Hu, Acta Mater. 45 (1997) 1837–1849.
[23] H.J. Grabke, M. Schutze, Oxidation of Intermetallics, Wiley-VCH Verlag GmbH, 1998.
[24] Y.G. Pan, J.F. Perales, E. Velo, L. Puigianer, Fuel 84 (2005) 1105–1109.
[25] E. Sasaoka, M. Sakamoto, T. Ichio, S. Kasaoka, Y. Sakata, Energy Fuels 7 (1993) 632–638.
[26] E. SasaoKa, M. Hatori, H. Yoshimura, C. Su, Ind. Eng. Chem. Res. 40 (2001) 2512–2517.
[27] J. Cermak, V. Rothova, Intermetallics 9 (2001) 403–408.
[28] Y. Wu, C. Su, W. Wang, H. Wang, Z. Shao, Int. J. Hydrogen Energy 37 (2012) 9287–9297.
[29] W. An, D. Gatewood, B. Dunlap, C.H. Turner, J. Power Sources 196 (2011) 4724–4728.
[30] X.C. Lu, J.H. Zhu, Z.H. Bi, Solid State Ionics 180 (2009) 265–270.
[31] J.C. Slater, J. Chem. Phys. 41 (1964) 3199–3205.
[32] K. Yaqoob, J.-C. Crivello, J.-M. Joubert, Inorg. Chem. 51 (2012) 3071–3078.
[33] V.V. Hoang, Phys. Rev. B 70 (2004) 134204–134214.
[34] O.V. Savin, N.N. Stepanova, Y.N. Akshentsev, D.P. Rodionov, Scr. Mater. 45 (2001) 883–888.
[35] B.S. Bokstein, S.Z. Bokstein, I.T. Spitsberg, Intermetallics 4 (1996) 517–523.
[36] J. Cermak, A. Gazda, V. Rothova, Intermetallics 11 (2003) 939–946.
[37] S. Pascarelli, F. Boscherini, S. Mobilio, K. Lawniczak-Jablonska, R. Kozubski, Phys. Rev. B 49 (1994) 14984–14990.
[38] A. Almazouzi, H. Numakura, M. Koiwa, K. Hono, T. Sakurai, Intermetallics 5 (1997) 37–43.
[39] R. Kozubski, J. Soltys, M.C. Cadeville, J. Phys. Condens. Matter 2 (1990) 3451–3458.
[40] E.W.D. Reca, C. Palmpillo, Acta Metall. 15 (1967) 1263–1268.
[41] J.K.V. Deen, F.V.D. Woude, Acta Metall. 29 (1981) 1255–1262.
[42] H.V.P. Nguyen, S.A. Song, D.-N. Park, H.C. Ham, J. Han, S.P. Yoon, M.R. Othman, J. Kim, Int. J. Hydrogen Energy 37 (2012) 16161–16167.
[43] S.A. Song, S.-C. Jang, J. Han, S.P. Yoon, S.W. Nam, I.-H. Oh, S.-G. Oh, Int. J. Hydrogen Energy 37 (2012) 19304–19311.
[44] J. Wang, M. Liu, Electrochem. Commun. 9 (2007) 2212–2217.
[45] D. Weaver, J. Winnick, J. Electrochem. Soc. 134 (1987) 2451–2458.
[46] S.Y. Hong, A.B. Anderson, Surf. Sci. 230 (1990) 175–183.
[47] S. Addepalli, N.P. Magtoto, J.A. Kelber, Langmuir 16 (2000) 8352–8359.
[48] J.B. Hansen, J. Electrochem. Soc. 11 (2008) B178–B180.
[49] J.A. Rodriguez, J. Phys. Chem. B 102 (1998) 5511–5519.
[50] J. Klower, G. Sauthoff, Mater. Corros. 48 (1997) 489–498.
[51] J. Wieckowska, Catal. Today 24 (1995) 405–465.
[52] X. Ren, L. Chang, F. Li, K. Xie, Fuel 89 (2010) 883–887.
[53] T.V. Reshetenko, S.R. Khairulin, Z.R. Ismagilov, V.V. Kuznetsov, Int. J. Hydrogen Energy 27 (2002) 387–394.
[54] J.D. White, F.R. Groves Jr., D.P. Harrison, Catal. Today 40 (1998) 47–57.
[55] S.P. Yoon, S.W. Nam, J. Han, T.-H. Lim, S.-A. Hong, S.-H. Hyun, Solid State Ionics 166 (2004) 1–11.
[56] C.Y. Yuh, J.R. Selman, AlChE J. 34 (1988) 1949–1958.
[57] C.H. Bartholomew, P.K. Agrawal, J.R. Katzer, Adv. Catal. 31 (1982) 135–242.
[58] H.P. Chen, R.K. Kalia, E. Kaxiras, G. Lu, Phys. Rev. Lett. 104 (2010) 155502–155506.